nature physics

Article

https://doi.org/10.1038/s41567-023-02027-1

Verification of the area law of mutual information in a quantum field simulator

Received: 11 July 2022

Accepted: 20 March 2023

Published online: 24 April 2023

Check for updates

Mohammadamin Tajik[1] ✉, Ivan Kukuljan[2,3], Spyros Sotiriadis[4], Bernhard Rauer[1,5], Thomas Schweigler[1], Federica Cataldini[1], João Sabino[1,6], Frederik Møller[1], Philipp Schüttelkopf[1], Si-Cong Ji[1], Dries Sels[7,8], Eugene Demler[9] & Jörg Schmiedmayer[1] ✉

The theoretical understanding of scaling laws of entropies and mutual information has led to substantial advances in the study of correlated states of matter, quantum field theory and gravity. Experimentally measuring von Neumann entropy in quantum many-body systems is challenging, as it requires complete knowledge of the density matrix, which normally requires the implementation of full state reconstruction techniques. Here we measure the von Neumann entropy of spatially extended subsystems in an ultracold atom simulator of one-dimensional quantum field theories. We experimentally verify one of the fundamental properties of equilibrium states of gapped quantum many-body systems—the area law of quantum mutual information. We also study the dependence of mutual information on temperature and on the separation between the subsystems. Our work represents a step towards employing ultracold atom simulators to probe entanglement in quantum field theories.

The study of quantum information measures is central to a wide range of areas in physics, from condensed matter and atomic physics to high energy physics and gravity[1–12]. Some of the most commonly studied quantities in quantum information are the (entanglement) entropy and the quantum mutual information. If a system described by a density matrix ϱ is composed of subsystems A and B, then the von Neumann (vN) entropy of subsystem A is defined as

$$S_A = -\mathrm{Tr}\left(\varrho_A \ln\left(\varrho_A\right)\right), \tag{1}$$

where $\varrho_A = \mathrm{Tr}_B(\varrho)$ is the reduced density matrix of subsystem A. If the state ϱ is pure ($\mathrm{Tr}\left(\varrho^2\right) = 1$), then the vN entropy is a measure of entanglement between A and B, thus called entanglement entropy, where $S_A = S_B$. For mixed states ($\mathrm{Tr}\left(\varrho^2\right) < 1$), the vN entropy captures both classical and quantum correlations, and it is no longer a good measure of entanglement. For mixed states, several other measures and witnesses of entanglement have been studied, with the positivity of the partial transpose criterion and quantum discord being prominent examples[1,13]. In cases where, rather than entanglement, the shared amount of information between two subsystems A and B is of interest, the quantum mutual information (MI)

$$I(A:B) = S_A + S_B - S_{A\cup B} \tag{2}$$

is a central object of study. It measures the total amount of correlation between the two subsystems, including all higher-order correlations for both pure and mixed states. For pure states, the value of the MI is equal to twice the entanglement entropy of one of the subsystems.

Information theory measures reveal one of the fundamental properties of quantum many-body systems, the area laws[3,14]. It was

[1]Vienna Center for Quantum Science and Technology (VCQ), Atominstitut, TU Wien, Vienna, Austria. [2]Max-Planck Institute of Quantum Optics, Garching, Germany. [3]Munich Center for Quantum Science and Technology (MCQST), Munich, Germany. [4]Dahlem Center for Complex Quantum Systems, Freie Universität Berlin, Berlin, Germany. [5]Laboratoire Kastler Brossel, ENS-Université PSL, CNRS, Sorbonne Université, Collège de France, Paris, France. [6]Instituto Superior Técnico, Universidade de Lisboa, Lisbon, Portugal. [7]Department of Physics, New York University, New York, NY, USA. [8]Center for Computational Quantum Physics, Flatiron Institute, New York, NY, USA. [9]Institute for Theoretical Physics, ETH Zurich, Zurich, Switzerland.
✉e-mail: amintajik.physics@gmail.com; schmiedmayer@atomchip.org

https://doi.org/10.1038/s41567-023-02027-1

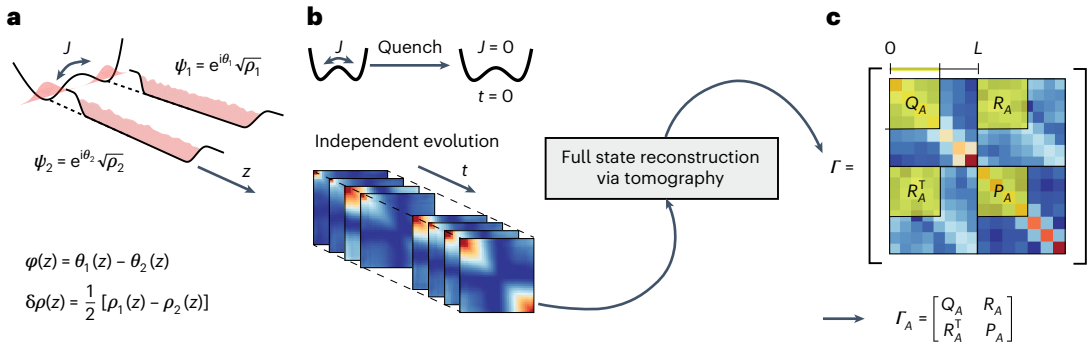

Fig. 1 | Schematic of the experimental protocol. a, The experimental protocol starts by cooling down a pair of tunnelling-coupled superfluids in a double-well potential with a finite single-particle tunnelling rate J, typically ~$2\pi \times 1$ Hz. The radial trapping frequency is $\omega_\perp = 2\pi \times 1.4$ kHz and the typical linear densities are $n_{1D} \approx 70\ \mu m^{-1}$. **b**, Immediately after the cooling process, the tunnelling rate is changed to zero in 2 ms. At $t = 0$, the two condensates are already uncoupled and their independent evolution following the TLL Hamiltonian starts. The measured phase correlations at different times are used to fit the full covariance matrix Γ. **c**, To calculate the vN entropy for a subsystem, $S(\Gamma_A)$, we use the correlations in that specific region (yellow shaded area). Note that Q, R and P have different units and the ranges of the colour axis are different. All tomography results are presented and discussed in Supplementary Information.

first noticed in gravitational physics that, surprisingly, the entropy of a black hole is proportional to the surface area of its event horizon and not its volume[11]. Interestingly, a similar property was found in quantum many-body systems: the vN entropy of ground states of systems with a gapped Hamiltonian scales with the surface area of the subsystem and not its volume[14]. Even more generally, thermal states of systems with a gapped Hamiltonian exhibit an area law of MI[15]. This means that the information shared between parts of a quantum many-body system is only considerable over a short distance, set by the correlation length. In particular, such a bound on the required information to model a many-body system provides the foundations for the overwhelming success of tensor network-based methods[2]. In contrast, it is known that critical systems described by conformal field theory exhibit a logarithmic scaling instead of the area law[9]. In thermal states, although the mutual information has an area or a log law, the vN entropy will exhibit a volume law, where it is proportional to the volume of the subsystem.

Extracting quantum information measures in quantum many-body systems has been the aim of several experiments[16–20]. Calculating the vN entropy requires access to the density matrix of the full system, ϱ, which usually requires a full state tomography in different experimental platforms. Instead of ϱ, several techniques have been developed to measure the purity, $\mathrm{Tr}(\varrho^2)$, which enables the calculation of second-order Rényi entropy, $S_2 = -\ln(\mathrm{Tr}(\varrho^2))$. These methods can be based on the interference of two identical copies of a quantum system[17] or randomized measurements on a single copy[20]. Note that, in these examples, the purity is directly measured but the full state is not reconstructed, so the calculation of vN entropy is not feasible.

Nevertheless, several optical lattice set-ups are able to measure the vN entropy, which is obtained either from a single-site reduced density matrix or as a classical thermodynamic entropy of the whole system[16,19]. In special cases, when the system is diagonal enough, even many-body vN entropy can be accessed[21]. However, the measurement of vN entropy between extended spatial subsystems has so far remained elusive, as has verification of the predicted area-law scaling of the MI.

In this article we address these challenges and study the scaling of the vN entropy and the MI with subsystem size in a continuous quantum many-body system. Our set-up is composed of a pair of tunnelling-coupled quasi-one-dimensional (1D) ultracold Bose gases (Fig. 1a), cooled down and trapped below an atom chip[22]. Along the longitudinal axis z, the clouds are confined in box-like potentials with hard walls, created by superposing magnetic and optical dipole potentials[23]. In one of the transverse directions, the atoms are trapped in a double-well potential, created by dressing with radiofrequency fields. The single-particle tunnelling rate J between the two condensates is adjusted by changing the amplitude of the radiofrequency fields[24].

To prepare a state in thermal equilibrium, we directly cool down an atomic cloud of ^{87}Rb in a strongly coupled double well, using the standard techniques of laser cooling and evaporative cooling[25]. The quantum fields describing each condensate can be written in phase–density representation as $\psi_n(z) = \exp(i\theta_n)\sqrt{\rho_n}$, with $n = 1, 2$. The spatially resolved relative phase between the two condensates, $\varphi(z) = \theta_1(z) - \theta_2(z)$, is extracted from interference images, taken 15.6 ms after releasing the atoms from the trap and letting them fall freely. In the limit of low energy excitations, the correlations of the relative phase are well described by the sine-Gordon Hamiltonian[26]. Expanding the interaction term in the case of high tunnelling rates leads to the massive Klein–Gordon (KG) Hamiltonian:

$$H_{\mathrm{KG}} = \int_0^L \mathrm{d}z \left[g_{1D}\delta\rho^2(z) + \frac{\hbar^2 n_{1D}}{4m}\left(\partial_z\varphi(z)\right)^2 + \hbar J n_{1D}\varphi^2(z) \right], \quad (3)$$

where L is the length of a system with uniform averaged 1D density n_{1D}, g_{1D} is the 1D interaction strength, m is the mass of an atom, and the relative density, $\delta\rho(z) = [\rho_1(z) - \rho_2(z)]/2$, is the conjugate field of the relative phase, fulfilling $[\varphi(z), \delta\rho(z')] = i\delta(z - z')$. A direct measurement of $\delta\rho(z)$ is unfeasible in our current experimental set-up. Hence, to reconstruct the full covariance matrix of the initial state

$$\Gamma = \begin{bmatrix} Q & R \\ R^{\mathrm{T}} & P \end{bmatrix} \quad (4)$$

we use a tomography procedure[27]. Here, $Q_{ij} = \langle\varphi(z_i)\varphi(z_j)\rangle$, $P_{ij} = \langle\delta\rho(z_i)\delta\rho(z_j)\rangle$ and $R_{ij} = \left\langle \frac{1}{2}\{\varphi(z_i), \delta\rho(z_j)\}\right\rangle$, with $i, j \in \{1, \ldots, N\}$, where z_i denotes different points on a discrete grid with N points. The upper limit for N is given by the resolution of the imaging system, which limits our access to higher momentum modes (larger than N) and enforces an ultraviolet (UV) cutoff.

To apply this tomographic method, we ramp up the barrier between the two strongly coupled condensates in 2 ms, and let them evolve independently in the uncoupled double well ($J = 0$). We then directly measure the phase–phase correlations for different evolution times after the quench. The post-quench dynamics follow the Tomonaga–Luttinger liquid (TLL) Hamiltonian. Over time, the initial eigenmodes of the relative density rotate into the phase quadrature and vice versa, enabling us to access the information about these eigenmodes by fitting the initial second-order correlation functions

https://doi.org/10.1038/s41567-023-02027-1

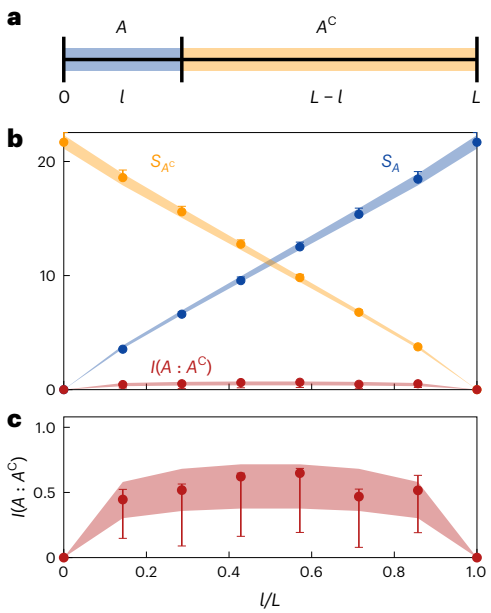

Fig. 2 | Area law of MI and volume law of vN entropy. a, A system of size $L = 49$ μm is divided into a subsystem A of length l and its complement subsystem of length $(L - l)$. **b**, The experimental results for $I(A{:}A^C)$, S_A and S_{A^C}, calculated based on $N = 7$ modes, are plotted as circles, with error bars representing the 95% confidence intervals obtained via bootstrapping[34] with 999 samples. The shaded areas show the 95% confidence interval for the theory predictions, considering the uncertainty in the estimated temperature and tunnelling rate J. **c**, Close-up of the measured MI from **b**.

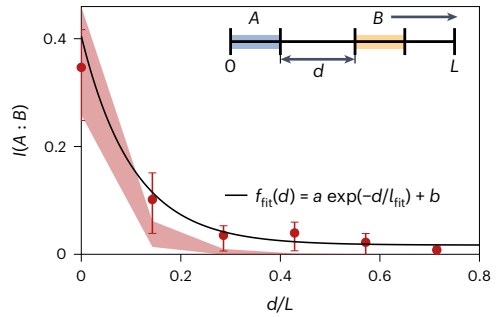

Fig. 3 | Shared information content between two spatially separated subsystems. We calculate the MI of two disjoint subsystems with the same length, $l/L = 0.15$, as a function of the distance between them, d. As demonstrated in the inset, while the subsystem A is kept fixed on the left edge of the system, B is shifted away to the other edge. Circles and shading represent experimental and theoretical data for $I(A{:}B)$, respectively (see Fig. 2 for more details on the error bars and shaded area). The solid black line is an exponential fit with $l_{fit} = 5.1$ μm. The finite bias b results from estimating a positive quantity, MI, using finite statistics.

of phase–density and density–density to the measured evolution of the phase–phase correlations in the momentum space. A thorough explanation of the reconstruction process is given in Methods, and the results are shown in Supplementary Information.

In the experiment, we prepare initial states that are thermal equilibrium states of the KG Hamiltonian. The quadratic form of this Hamiltonian, as shown in equation (3), implies that the prepared initial states are Gaussian. After a fast quench of J to zero, the initial state evolves under another quadratic Hamiltonian, ensuring that the state remains Gaussian under evolution[28]. To confirm Gaussianity, we measure the normalized, averaged connected fourth-order correlation function, $M^{(4)}$, and show that the higher-order correlations are negligible. Note that the tomography process does not include any restrictions regarding the Gaussianity of the reconstructed state.

Having Gaussian states greatly simplifies the calculation of the quantum information measures—an otherwise highly non-trivial task in quantum field theory[29]. Gaussian states are fully described by their covariance matrix Γ. Its symplectic spectrum is obtained by diagonalizing $i\mathcal{J}\Gamma$, where $\mathcal{J} = \begin{bmatrix} 0 & I \\ -I & 0 \end{bmatrix}$ is the symplectic unit. The symplectic spectrum consists of pairs $\pm\gamma_n$, $n \in \{1, \ldots, N\}$. It encodes the complete information that is contained in the covariance matrix[14]. Consequently, it can be used to reconstruct the full density matrix of the state and the measures of quantum information. In particular, the vN entropy is given by

$$S(\Gamma) = \sum_{n=1}^{N} \left[\left(\gamma_n + \frac{1}{2}\right) \ln\left(\gamma_n + \frac{1}{2}\right) - \left(\gamma_n - \frac{1}{2}\right) \ln\left(\gamma_n - \frac{1}{2}\right) \right]. \quad (5)$$

For non-Gaussian states, neglecting higher-order correlations and estimating the vN entropy based on the covariance matrix gives a lower bound to the actual entropy[30].

Having the reconstructed initial covariance matrix at hand, we use equation (5) to calculate the vN entropy of any subsystem A, $S_A(\Gamma_A)$ (Fig. 1c). Using equation (2), the MI between two subsystems A and B is calculated. To observe the scaling of the vN entropy and the MI, we calculate the vN entropy of subsystems with different lengths and consecutively the MI with the complement subsystems, as illustrated in Fig. 2a. As expected for thermal states, the vN entropy is in the volume-law regime, depending linearly on the size of the subsystem (Fig. 2b and Extended Data Fig. 1a). Measuring the vN entropy allows us to study the scaling of the mutual information. We find an area law for MI, with a plateau forming in the bulk of the system (Fig. 2c and Extended Data Fig. 1b). Our results represent an experimental verification of one of the elementary features of quantum many-body systems[15].

We continue by studying the dependence of MI on the distance between two subsystems. In this case, we calculate the MI of two subsystems A and B, separated by a gap of length d. The results are presented in Fig. 3. As expected, the MI decreases as the two subsystems get further apart. We can extract a decay length by fitting an exponential function to the experimental data. The fitted decay length, $l_{fit} = 5.1\ (3.7, 8)$ μm agrees with the correlation length $l_c = 6.8\ (6, 7.7)$ μm calculated based on the experimental parameters (Methods). The intervals in parentheses represent the 95% confidence intervals obtained via bootstrapping.

For the typical temperatures of our experiment, the vN entropy depends linearly on the temperature. The linear dependence changes to a logarithmic dependence by introducing a finite UV cutoff, as shown in the inset of Fig. 4 (dashed lines). As the temperature increases, the symplectic eigenvalues grow, and the calculated entropy using a finite number of modes saturates. The MI, however, regardless of the UV cutoff, reaches a finite asymptotic value given by the classical correlations[31]. Reducing the number of modes reduces the asymptotic value due to the limited available information in the modes taken into account, as presented in the inset of Fig. 4 (solid lines). In Fig. 4, the measured vN entropy and MI for three different temperatures are presented, along with theoretical predictions. The measurements agree with the theory calculated for the extracted parameters and $N = 7$ lowest modes.

It is important to stress that the only assumption we make to calculate the vN entropy and the MI is that the post-quench dynamics follow a TLL Hamiltonian, which has been confirmed in a previous work[28]. Our measurements do not rely on any assumption related to the Gaussianity of the initial state. We rather confirm that the initial

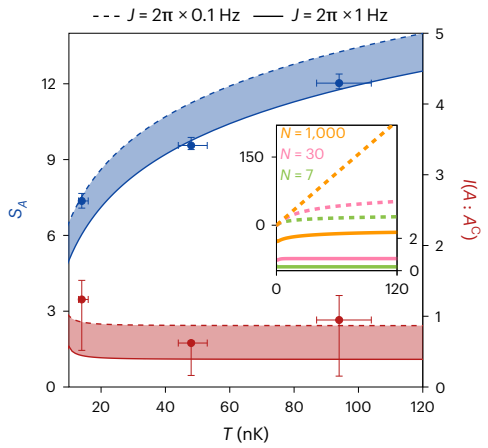

Fig. 4 | Temperature dependence of MI and vN entropy. The circles represent experimental data for S_A (left axis) and $I(A{:}A^C)$ (right axis) with $N = 7$ for measurements with three different temperatures, but otherwise similar parameters. The size of the subsystem A is $l/L = 0.4$ (Fig. 2a). The error bars show the 95% confidence intervals achieved via bootstrapping with 999 samples. The shaded areas represent the calculations based on the theoretical model for different tunnelling rates, between $J = 2\pi \times 0.1$ Hz (dashed lines) and $2\pi \times 1$ Hz (solid lines). Inset: theoretical predictions for S_A (left axis) and $I(A{:}A^C)$ (right axis) for three different values of N, for $J = 2\pi \times 0.4$ Hz, without considering the effect of finite optical resolution (Methods).

state is Gaussian by measuring the higher-order correlations. Even for non-Gaussian initial states, our results would represent a lower bound to the entropy of the full state.

The results presented here are a step towards the more ambitious goal of measuring many-body entanglement in a continuous 1D quantum system. Reconstruction of the full covariance matrix enables us to calculate any entanglement measure applicable to both pure and mixed states, such as logarithmic negativity. However, there are two main limiting factors preventing us from detecting the entanglement. The entanglement can only be detected if a sufficient number of momentum modes are measured whose mode occupation numbers are close to the ground state. In our current experiments, the non-zero temperature (10–100 nK) of the Bose gas keeps the occupation numbers of the lower momentum modes too high above the value of the ground state. At the same time, the finite optical resolution introduces a soft cutoff that not only prevents us from measuring higher momentum modes but also modifies the lower modes that can be measured. Improving any of these two aspects would make the measurement of the entanglement possible.

Another promising direction for future work is to go beyond quadratic models and detect entanglement in an interacting model. It has already been demonstrated that atom chip experiments can successfully simulate the sine-Gordon model, and higher-order correlation functions can be measured[26]. Developing a tomography procedure for this setting would give us access to entanglement properties in interacting many-body quantum systems[32,33].

Online content

Any methods, additional references, Nature Portfolio reporting summaries, source data, extended data, supplementary information, acknowledgements, peer review information; details of author contributions and competing interests; and statements of data and code availability are available at https://doi.org/10.1038/s41567-023-02027-1.

References

1. Horodecki, R., Horodecki, P., Horodecki, M. & Horodecki, K. Quantum entanglement. *Rev. Mod. Phys.* **81**, 865–942 (2009).
2. Orús, R. A practical introduction to tensor networks: matrix product states and projected entangled pair states. *Ann. Phys.* **349**, 117–158 (2014).
3. Schuch, N., Wolf, M. M., Verstraete, F. & Cirac, J. I. Entropy scaling and simulability by matrix product states. *Phys. Rev. Lett.* **100**, 030504 (2008).
4. Abanin, D. A., Altman, E., Bloch, I. & Serbyn, M. Colloquium: many-body localization, thermalization and entanglement. *Rev. Mod. Phys.* **91**, 021001 (2019).
5. Senthil, T. Symmetry-protected topological phases of quantum matter. *Annu. Rev. Condens. Matter Phys.* **6**, 299–324 (2015).
6. Callan, C. & Wilczek, F. On geometric entropy. *Phys. Lett. B* **333**, 55–61 (1994).
7. Holzhey, C., Larsen, F. & Wilczek, F. Geometric and renormalized entropy in conformal field theory. *Nucl. Phys. B* **424**, 443–467 (1994).
8. Srednicki, M. Entropy and area. *Phys. Rev. Lett.* **71**, 666–669 (1993).
9. Calabrese, P. & Cardy, J. Entanglement entropy and quantum field theory. *J. Stat. Mech. Theory Exp.* **2004**, 06002 (2004).
10. Calabrese, P. & Cardy, J. Entanglement entropy and conformal field theory. *J. Phys. A Math. Theor.* **42**, 504005 (2009).
11. Polchinski, J. in *New Frontiers in Fields And Strings* (eds Polchinski, J. et al.) 353–397 (World Scientific, 2017); https://doi.org/10.1142/9789813149441_0006
12. Ryu, S. & Takayanagi, T. Holographic derivation of entanglement entropy from the anti-de Sitter space/conformal field theory correspondence. *Phys. Rev. Lett.* **96**, 181602 (2006).
13. Modi, K., Brodutch, A., Cable, H., Paterek, T. & Vedral, V. The classical-quantum boundary for correlations: discord and related measures. *Rev. Mod. Phys.* **84**, 1655–1707 (2012).
14. Eisert, J., Cramer, M. & Plenio, M. B. Colloquium: area laws for the entanglement entropy. *Rev. Mod. Phys.* **82**, 277–306 (2010).
15. Wolf, M. M., Verstraete, F., Hastings, M. B. & Cirac, J. I. Area laws in quantum systems: mutual information and correlations. *Phys. Rev. Lett.* **100**, 070502 (2008).
16. Luo, L., Clancy, B., Joseph, J., Kinast, J. & Thomas, J. E. Measurement of the entropy and critical temperature of a strongly interacting Fermi gas. *Phys. Rev. Lett.* **98**, 080402 (2007).
17. Islam, R. et al. Measuring entanglement entropy in a quantum many-body system. *Nature* **528**, 77–83 (2015).
18. Omran, A. et al. Microscopic observation of Pauli blocking in degenerate fermionic lattice gases. *Phys. Rev. Lett.* **115**, 263001 (2015).
19. Cocchi, E. et al. Measuring entropy and short-range correlations in the two-dimensional Hubbard model. *Phys. Rev. X* **7**, 031025 (2017).
20. Brydges, T. et al. Probing Rényi entanglement entropy via randomized measurements. *Science* **364**, 260–263 (2019).
21. Evrard, B., Qu, A., Dalibard, J. & Gerbier, F. Observation of fragmentation of a spinor Bose-Einstein condensate. *Science* **373**, 1340–1343 (2021).
22. Folman, R. et al. Controlling cold atoms using nanofabricated surfaces: atom chips. *Phys. Rev. Lett.* **84**, 4749–4752 (2000).
23. Tajik, M. et al. Designing arbitrary one-dimensional potentials on an atom chip. *Opt. Exp.* **27**, 33474–33487 (2019).
24. Schumm, T. et al. Matter-wave interferometry in a double well on an atom chip. *Nat. Phys.* **1**, 57–62 (2005).
25. Rauer, B. et al. Cooling of a one-dimensional Bose gas. *Phys. Rev. Lett.* **116**, 030402 (2016).
26. Schweigler, T. et al. Experimental characterization of a quantum many-body system via higher-order correlations. *Nature* **545**, 323–326 (2017).
27. Gluza, M. et al. Quantum read-out for cold atomic quantum simulators. *Commun. Phys.* **3**, 12 (2020).

28. Schweigler, T. et al. Decay and recurrence of non-Gaussian correlations in a quantum many-body system. *Nat. Phys.* **17**, 559–563 (2021).
29. Serafini, A. *Quantum Continuous Variables: a Primer of Theoretical Methods* (CRC Press, 2017).
30. Eisert, J. & Wolf, M. M. in *Quantum Information with Continuous Variables of Atoms and Light* (eds Cerf, N. J. et al.) 23–42 (World Scientific, 2007); https://doi.org/10.1142/9781860948169_0002
31. Katsinis, D. & Pastras, G. An inverse mass expansion for the mutual information in free scalar qft at finite temperature. *J. High Energy Phys.* **2020**, 91 (2020).
32. Kukuljan, I., Sotiriadis, S. & Takacs, G. Correlation functions of the quantum sine-Gordon model in and out of equilibrium. *Phys. Rev. Lett.* **121**, 110402 (2018).
33. Emonts, P. & Kukuljan, I. Reduced density matrix and entanglement of interacting quantum field theories with Hamiltonian truncation. *Phys. Rev. Res* **4**, 033039 (2022).
34. Efron, B. & Tibshirani, R. Bootstrap methods for standard errors, confidence intervals and other measures of statistical accuracy. *Stat. Sci.* **1**, 54–75 (1986).

Publisher's note Springer Nature remains neutral with regard to jurisdictional claims in published maps and institutional affiliations.

Springer Nature or its licensor (e.g. a society or other partner) holds exclusive rights to this article under a publishing agreement with the author(s) or other rightsholder(s); author self-archiving of the accepted manuscript version of this article is solely governed by the terms of such publishing agreement and applicable law.

© The Author(s), under exclusive licence to Springer Nature Limited 2023

Methods

Experimental realization and measurements

We realized a pair of strongly tunnelling-coupled 1D superfluids by cooling down ^{87}Rb atoms in a double-well potential in an atom chip set-up. The initial state was prepared by cooling the atoms directly into a double-well potential. The initial state in this case is a thermal equilibrium state with typical temperatures of 30–120 nK and linear atomic densities of ~70 μm^{-1} in a box-like potential with length ~50 μm.

To achieve lower effective temperatures, we first cooled down the atoms in a dressed single-well potential, where the first excited state was in the vacuum state. Slowly splitting the cloud into two parts maps the ground state and the first excited state to two states with a smaller energy gap and symmetric and antisymmetric wavefunctions. The resulting prethermalized state has a lower effective temperature in the antisymmetric modes (relative degrees of freedom)[35]. This method has been deployed in the measurement with effective temperature $T_{\mathrm{eff}} = 14$ nK presented in Fig. 4 and Extended Data Fig. 1.

To probe the system, we turned off all the traps and let the atoms fall freely for 15.6 ms. We measured the projected 2D atomic density distributions via absorption imaging, from which we extracted the relative phase between the two condensates for different points along the 1D direction, z. Due to the destructive nature of the imaging process, we repeated the measurement hundreds of times to accumulate statistics. Thus, all the expectation values calculated are obtained through ensemble averaging.

Quantum field simulation using coupled quasi-1D superfluids

As has been discussed in several earlier works (for example, refs. 26,28,36), low-energy excitations of coupled parallel 1D gases of weakly interacting atoms can be utilized as a quantum-field simulator of the sine-Gordon Hamiltonian:

$$H_{\mathrm{sG}} = \int_0^L \mathrm{d}z \left[g_{1\mathrm{D}} \delta\rho^2 + \frac{\hbar^2 n_{1\mathrm{D}}}{4m} (\partial_z \varphi)^2 - 2\hbar J n_{1\mathrm{D}} \cos(\varphi) \right]. \tag{6}$$

This model describes the relative phase, φ, and the relative density fluctuations of two superfluids (Fig. 1a). These two fields are the canonical conjugate of one another, that is, $[\varphi(z), \delta\rho(z')] = -\mathrm{i}\delta(z - z')$. In equation (6), m is the atomic mass, $n_{1\mathrm{D}}$ is the uniform atomic density of the condensates, $g_{1\mathrm{D}}$ is the inter-atomic interaction, and J is the single-particle tunnelling rate.

For sufficiently cold gases in the strong coupling regime, that is, when the phase coherence length

$$\lambda_{\mathrm{T}} = \frac{2\hbar^2 n_{1\mathrm{D}}}{m k_{\mathrm{B}} T} \tag{7}$$

is larger than the healing length of the relative phase (correlation length)

$$l_{\mathrm{C}} = \sqrt{\frac{\hbar}{4mJ}}, \tag{8}$$

the cosine term in equation (6) can be expanded to second order and be approximated by the quadratic KG model. Introducing the sound velocity c, Luttinger parameter K and the KG quasi-particle mass, M, given in terms of the microscopic parameters by

$$c = \sqrt{\frac{g_{1\mathrm{D}} n_{1\mathrm{D}}}{m}} \tag{9}$$

$$K = \frac{\hbar\pi}{2} \sqrt{\frac{n_{1\mathrm{D}}}{m g_{1\mathrm{D}}}} \tag{10}$$

$$M = 2m \sqrt{\frac{\hbar J}{g_{1\mathrm{D}} n_{1\mathrm{D}}}}, \tag{11}$$

the KG Hamiltonian can be written as

$$H_{\mathrm{KG}} = \frac{\hbar c}{2} \int_0^L \mathrm{d}z \left[\frac{\pi}{K} \delta\rho^2(z) + \frac{K}{\pi} (\partial_z \varphi(z))^2 \right] + \frac{M^2 c^4}{2\hbar c} \int_0^L \mathrm{d}z \, \frac{K}{\pi} \varphi^2(z). \tag{12}$$

Note that the first two terms in equation (12) are the TLL Hamiltonian. In Supplementary Table 1, the relevant parameters for each measurement are listed, where $\omega_{\mathrm{M}} = Mc^2/\hbar$ is the KG mass in units of angular frequency.

Reconstruction of the initial full covariance matrix

To extract the full covariance matrix that characterizes the state of the system, we use the quantum tomography method developed in ref. 27. Given that only one of the two canonical variables (the phase) is accessible through experimental measurements, its canonically conjugate variable (the density fluctuations) can be accessed indirectly by letting the system evolve under a harmonic Hamiltonian with known mode frequencies and measuring the phase at different times. For each of the harmonic modes, the dynamics correspond to a rotation in phase space, so that, over time, the initial density variance turns into phase variance and vice versa. We can thus fully reconstruct the initial covariance matrix from phase measurements at a sufficiently large number of different times. This reconstruction is done by first going to Fourier space, where the modes evolve independently, and then fitting the data for the time evolution of the phase covariance of each mode to the known functions expressing this data in terms of the initial phase and density correlations.

However, one mode needs special treatment: the zero mode, that is, the mode corresponding to zero momentum, therefore zero energy. This mode does not rotate in phase space; instead, it moves at a constant velocity. This means that the zero-mode phase variance does not oscillate in time but grows as a quadratic function of time instead, an effect known as phase diffusion[37]. Moreover, because of the compactified nature of the phase field, which means that phases differing by 2π should be considered identical, even though the phase grows in time with no bound, measurements can only observe its growth within the interval [−π, +π]. Therefore, the estimation of the initial phase and density correlations of the zero mode is different from that of the others. For the zero mode, we fit a quadratic function instead of an oscillatory function of time, and we restrict the fit to times before reaching the upper bound due to compactification.

More specifically, the dynamics are chosen to follow the TLL model with Hamiltonian

$$H_{\mathrm{TLL}} = \int_0^L \mathrm{d}z \left[g_{1\mathrm{D}} (\delta\rho(z))^2 + \frac{\hbar^2 n_{1\mathrm{D}}}{4m} (\partial_z \varphi(z))^2 \right]. \tag{13}$$

For a hard-wall box trap, the vanishing of the particle current at the edges of the system means that the effective boundary conditions are of Neumann type $\partial_z\varphi(x=0) = \partial_z\varphi(x=L) = 0$. In this case, using the cosine eigenfunctions

$$f_n^{\varphi}(z) = \begin{cases} 2\left(n\hbar\pi \sqrt{\frac{n_{1\mathrm{D}}}{g_{1\mathrm{D}} m}}\right)^{-1/2} \cos(n\frac{\pi}{L} z), & n > 0 \\ 1, & n = 0 \end{cases}$$

$$f_n^{\delta\rho}(z) = \begin{cases} -\frac{1}{L}\left(n\hbar\pi \sqrt{\frac{n_{1\mathrm{D}}}{g_{1\mathrm{D}} m}}\right)^{1/2} \cos(n\frac{\pi}{L} z), & n > 0 \\ -\frac{1}{L}, & n = 0 \end{cases}, \tag{14}$$

the Hamiltonian can be diagonalized in terms of cosine Fourier modes:

$$H = \frac{\hbar u}{2} \delta\rho_0^2 + \sum_{n=1}^{\infty} \frac{\hbar\omega_n}{2} [\delta\rho_n^2 + \varphi_n^2], \tag{15}$$

with

$$u = 2g_{1D}/\hbar L \tag{16}$$

$$\omega_n = ck_n. \tag{17}$$

Furthermore

$$k_n = n\pi/L \tag{18}$$

$$c = \sqrt{g_{1D}n_{1D}/m} \tag{19}$$

$$g_{1D} = \hbar\omega_\perp a_s \frac{2 + 3a_s n_{1D}}{(1 + 2a_s n_{1D})}, \tag{20}$$

where c is the speed of sound, g_{1D} is the density-broadened 1D interaction strength[38], $a_s = 5.2$ nm is the 3D scattering length[39] and $m = 1.44 \times 10^{-25}$ kg is the mass of a ^{87}Rb atom.

As mentioned before and reflected in the TLL Hamiltonian in Fourier space (equation (15)), we have to treat the zero mode separately. We begin with the harmonic part of the Hamiltonian ($n > 0$) where the time evolution of the modes is given by

$$\delta\rho_n(t) = \delta\rho_n(0)\cos(\omega_n t) + \varphi_0(0)\sin(\omega_n t) \tag{21}$$

$$\varphi_n(t) = \varphi_0(0)\cos(\omega_n t) - \delta\rho_n(0)\sin(\omega_n t). \tag{22}$$

In the experiment, we use matter interferometry to measure the spatially resolved relative phase between two superfluids, from which a referenced second-order correlation is calculated for each time step:

$$\Phi^2_{ab}(t) = \langle(\varphi(z_a, t) - \varphi(z_0, t))(\varphi(z_b, t) - \varphi(z_0, t))\rangle. \tag{23}$$

Note that subtracting the phase of an arbitrary reference position z_0 will only remove the zero mode and does not affect any of the higher modes.

Expanding Φ^2 with the eigenfunctions of equation (14), gives

$$\Phi^2_{ab}(t) = \sum_{j,k=1}^{N} f^{a,b}_{j,k} \langle\varphi_j(t)\varphi_k(t)\rangle, \tag{24}$$

where

$$f^{a,b}_{j,k} = \left(f^{\phi}_j(z_a) - f^{\phi}_j(z_0)\right)\left(f^{\phi}_k(z_b) - f^{\phi}_k(z_0)\right). \tag{25}$$

Using the equation of motion in equation (22), and defining $\tilde{Q}_{jk} = \langle\varphi_j(0)\varphi_k(0)\rangle$, $\tilde{R}_{jk} = \left\langle \frac{1}{2}\{\varphi_j(0), \delta\rho_k(0)\}\right\rangle$ and $\tilde{P}_{jk} = \langle\delta\rho_j(0)\delta\rho_k(0)\rangle$, we obtain

$$\begin{aligned}\Phi^2_{ab}(t) = &\sum_{j,k=1}^{N} f^{a,b}_{j,k}\cos(\omega_j t)\cos(\omega_k t)\tilde{Q}_{jk} \\ &+ \sum_{j,k=1}^{N}(-f^{a,b}_{j,k} - f^{a,b}_{j,k})\cos(\omega_j t)\sin(\omega_k t)\tilde{R}_{jk} \\ &+ \sum_{j,k=1}^{N} f^{a,b}_{j,k}\sin(\omega_j t)\sin(\omega_k t)\tilde{P}_{jk}\end{aligned} \tag{26}$$

Equation (26) stands in the heart of the tomography process: the goal is to find the elements of $\tilde{Q}$, $\tilde{R}$ and $\tilde{P}$ using an optimization process. Note that the left-hand side is calculated using phase profiles measured in the experiment and, in the right hand side, $f^{a,b}_{j,k}$ and ω_j can be calculated from the experimental parameters, as shown in equations (14) and (17), respectively. The results are presented in Supplementary Information. For a more detailed explanation of the tomography process, please refer to ref. 27.

Unlike all higher modes, the zero mode, which corresponds to the constant in space eigenfunction, is not a harmonic oscillator mode of the TLL Hamiltonian (equation (13)). This is because only one of the canonical variables, $\delta\rho_0$, is present in the Hamiltonian for the zero mode. As a result, the time evolution of the zero mode is given by

$$\delta\rho_0(t) = \delta\rho_0(0) = \text{const.} \tag{27}$$

$$\varphi_0(t) = -u\delta\rho_0(0)t + \varphi_0(0), \tag{28}$$

which means that the phase variance grows with time as

$$\left\langle\varphi_0(t)^2\right\rangle = \left\langle\varphi_0^2\right\rangle_{t=0} - \left\langle\{\varphi_0, \delta\rho_0\}\right\rangle_{t=0}ut + \left\langle\delta\rho_0^2\right\rangle_{t=0}u^2t^2. \tag{29}$$

However, because of the compactified nature of the phase field, its zero mode component φ_0 is not a well-defined, measurable operator. Only imaginary exponentials of the form $e^{in\varphi_0}$ for integer n are well-defined. Nevertheless, under the assumption that the initial state is Gaussian in terms of the zero mode (as also for all other modes too) and given that it remains Gaussian under the dynamics following from H_{TLL}, we can derive the zero-mode variance from the mean value of $e^{in\varphi_0}$ using the cumulant expansion formula for the special case of Gaussian random variables:

$$\langle\exp(i\varphi_0)\rangle = \exp\left(i\langle\varphi_0\rangle - \left\langle\varphi_0^2\right\rangle/2\right). \tag{30}$$

From the above, we find

$$\left\langle\varphi_0^2\right\rangle = -2\log|\langle\exp(i\varphi_0)\rangle|. \tag{31}$$

Therefore, to extract the zero-mode part of the covariance matrix $\left\langle\varphi_0^2\right\rangle_{t=0}$, $\left\langle\delta\rho_0^2\right\rangle_{t=0}$ and $\left\langle\{\varphi_0, \delta\rho_0\}\right\rangle_{t=0}$ in the initial state we calculate the zero-mode variance of the phase at each time from equation (30) and fit this with the theoretical equation (31).

Having the covariance matrix in the Fourier space for the first N modes, we use a discrete Fourier transformation based on the eigenfunctions (equation (14)) to calculate the covariance matrix Γ in real space. We chose the cutoff based on the reconstructed occupation numbers. We only take into account modes with physical (positive) occupation numbers. This covariance matrix is used to calculate vN entropy and MI, as discussed in the main text and Fig. 1c.

Covariance matrix of KG model in thermal equilibrium

The theory predictions in our work are calculated based on the covariance matrix of the thermal equilibrium states of KG model (equation (3)), which is given by[40]

$$\begin{aligned}Q_{ij} = &\frac{\pi}{2KL}\frac{\hbar c}{Mc^2}\coth\left(\frac{Mc^2}{2k_B T}\right) \\ &+ \frac{\pi}{KL}\sum_{n=1}^{N}\frac{\hbar c}{\epsilon_n}\coth\left(\frac{\epsilon_n}{2k_B T}\right)\cos(k_n z_i)\cos(k_n z_j)\end{aligned} \tag{32}$$

$$R_{ij} = 0 \tag{33}$$

$$\begin{aligned}P_{ij} = &\frac{K}{2\pi L}\frac{Mc^2}{\hbar c}\coth\left(\frac{Mc^2}{2k_B T}\right) \\ &+ \frac{K}{\pi L}\sum_{n=1}^{N}\frac{\epsilon_n}{\hbar c}\coth\left(\frac{\epsilon_n}{2k_B T}\right)\cos(k_n z_i)\cos(k_n z_j)\end{aligned} \tag{34}$$

with the dispersion relation $\epsilon_n = \sqrt{\hbar^2 k_n^2 c^2 + M^2 c^4}$. Here, M is the KG mass, L is the system size, K is the Luttinger parameter, T is the temperature, N is the UV cutoff, and the rest of the parameters are defined as before. The next section will explain how M and T are estimated based on the measured data. To include the effect of the finite imaging resolution,

we convolve the theoretical calculations with a Gaussian point-spread function with a standard deviation $\sigma_{PSF} \approx 3\,\mu m$ (ref. 38; see next section).

Estimation of the temperature and KG mass

To compute theoretical predictions for the mutual information in the initial state based on the assumption that these are the thermal states of the KG model, we need to estimate two effective parameters—the mass and the temperature. We do this by fitting the results of the tomographic reconstruction for the mode variances to those corresponding to KG thermal states. Given that the modes are decoupled from each other both initially and throughout the tomography dynamics, estimation of the KG mode frequency can be done independently for each mode. Having estimated the mode frequencies, we can then verify whether they follow the theoretical dispersion relation of the KG model and extract the corresponding mass parameter by a fit.

The relation between the post-quench quadratures and the initial (pre-quench) KG state with mode occupation number N_{0n} is given by

$$\langle \varphi_n^2 \rangle = \frac{\omega_n}{\omega_{0n}} \left(N_{0n} + \frac{1}{2} \right) \tag{35}$$

$$\langle \delta\rho_n^2 \rangle = \frac{\omega_{0n}}{\omega_n} \left(N_{0n} + \frac{1}{2} \right), \tag{36}$$

where ω_{0n} and ω_n are the pre- and post-quench mode frequencies, respectively. Both $\langle \varphi_n^2 \rangle$ and $\langle \delta\rho_n^2 \rangle$ are achieved via tomography, and ω_n is given by equation (17). From equations (35) and (36) we can calculate both ω_{0n} and N_{0n}:

$$N_{0n} = \sqrt{\langle \varphi_n^2 \rangle \langle \delta\rho_n^2 \rangle} - \frac{1}{2} \tag{37}$$

$$\omega_{0n} = \omega_n \sqrt{\frac{\langle \delta\rho_n^2 \rangle}{\langle \varphi_n^2 \rangle}}. \tag{38}$$

Assuming the initial state is thermal, we use the following fit function to extract the temperature, $T = (\beta k_B)^{-1}$:

$$N_{0n}^{\text{fit}} = \exp\left(-k_n^2 \sigma_{PSF}^2/2\right) \left(\frac{1}{\exp(\hbar\omega_{0n}\beta) - 1} + \frac{1}{2} \right) - \frac{1}{2}. \tag{39}$$

Note that we also introduce the effect of the imaging system by multiplying the modes with a Gaussian point-spread function with width σ_{PSF}, which corresponds to a convolution with a Gaussian point-spread function in the real space[38]. To extract the KG mass, we fit the KG dispersion relation,

$$\omega_{0n}^{\text{fit}} = \sqrt{c^2 k_n^2 + M^2 c^4/\hbar^2} \tag{40}$$

to the calculated ω_{0n}.

Data availability

The experimental raw data containing all the information required to extract and calculate the results presented in Figs. 2–4 and Extended Data Fig. 1 are available in ref. 41. Sample code for calculating absorption images from raw data is also available there. All other data are available from the corresponding authors upon reasonable request. Source data are provided with this paper.

References

35. Gring, M. et al. Relaxation and prethermalization in an isolated quantum system. *Science* **337**, 1318–1322 (2012).
36. Rauer, B. et al. Recurrences in an isolated quantum many-body system. *Science* **360**, 307–310 (2018).
37. Berrada, T. et al. Integrated Mach-Zehnder interferometer for Bose-Einstein condensates. *Nat. Commun.* **4**, 2077 (2013).
38. Schweigler, T. *Correlations and Dynamics of Tunnel-Coupled One-Dimensional Bose Gases*. PhD thesis, Techniche Universität Wien (2019); https://doi.org/10.34726/hss.2019.63111
39. van Kempen, E. G., Kokkelmans, S. J., Heinzen, D. J. & Verhaar, B. J. Interisotope determination of ultracold rubidium interactions from three high-precision experiments. *Phys. Rev. Lett.* **88**, 093201 (2002).
40. Le Bellac, M. *Thermal Field Theory*. *Cambridge Monographs on Mathematical Physics* (Cambridge Univ. Press, 1996); https://doi.org/10.1017/CBO9780511721700
41. Tajik, M. et al. Raw data to 'Experimental verification of the area law of mutual information in quantum field theory'. *Zenodo* https://doi.org/10.5281/zenodo.6851336 (2022).

Acknowledgements

We thank M. Gluza, J. Eisert, I. Cirac, I. Mazets and S. Erne for helpful discussions. This work is supported by the DFG/FWF Research Unit FOR 2724 'Thermal machines in the quantum world', the FQXi programme on 'Information as fuel', and DFG/FWF CRC 1225, 'Isolated quantum systems and universality in extreme conditions (ISOQUANT)'. The Flatiron Institute is a division of the Simons Foundation. E.D. acknowledges support from ARO grant no. W911NF-20-1-0163. The work of I.K. was supported by the Max-Planck-Harvard Research Center for Quantum Optics (MPHQ). F.C., F.M. and J. Sabino acknowledge support from the Austrian Science Fund (FWF) in the framework of the Doctoral School on Complex Quantum Systems (CoQuS). J. Sabino acknowledges support by the Fundação para a Ciência e Tecnologia, Portugal (PD/BD/128641/2017). T.S. acknowledges support from the Max Kade Foundation through a postdoctoral fellowship. B.R. acknowledges support by the European Union's Horizon 2020 research and innovation programme under Marie Skłodowska-Curie grant agreement no. 888707. D.S. is partially supported by AFOSR (grant no. FA9550-21-1-0236) and NSF (grant no. OAC-2118310). S.S. acknowledges support by the European Union's Horizon 2020 research and innovation programme under Marie Skłodowska-Curie grant agreement no. 101030988 and by the Slovenian Research Agency (ARRS) under a QTE grant (no. N1-0109).

Author contributions

M.T. and B.R. performed the experiment with contributions by T.S., F.C., S.-C.J., J. Sabino, F.M. and P.S. M.T. analysed the experimental data. I.K., S.S. and M.T. provided the theoretical methodology and calculations, with helpful suggestions from D.S. J. Schmiedmayer and E.D. provided scientific guidance on experimental and theoretical questions. J. Schmiedmayer conceived the experiment. All authors contributed to the interpretation of the data and to the writing of the manuscript.

Competing interests

The authors declare no competing interests.

Additional information

Extended data is available for this paper at https://doi.org/10.1038/s41567-023-02027-1.

Supplementary information The online version contains supplementary material available at https://doi.org/10.1038/s41567-023-02027-1.

Correspondence and requests for materials should be addressed to Mohammadamin Tajik or Jörg Schmiedmayer.

Peer review information *Nature Physics* thanks the anonymous reviewers for their contribution to the peer review of this work.

Reprints and permissions information is available at www.nature.com/reprints.

https://doi.org/10.1038/s41567-023-02027-1

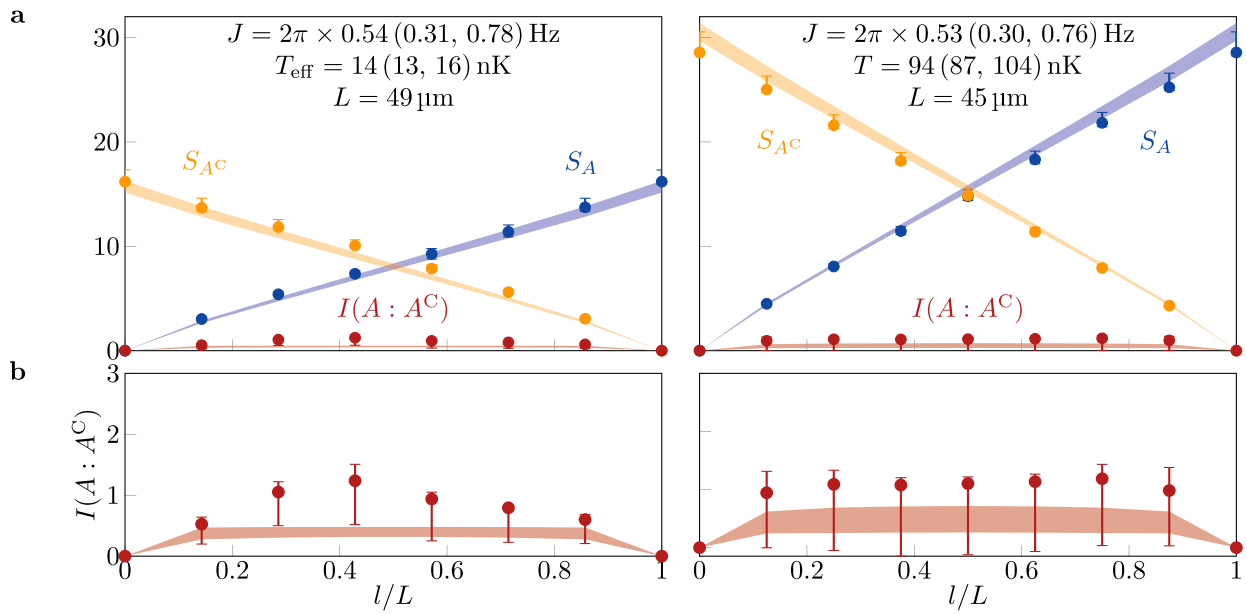

Extended Data Fig. 1 | Additional results for area law of MI and volume law of vN entropy. a, Experimental results for $I(A{:}A^C)$, S_A, and S_{A^C}, calculated based on $N = 7$ modes (left) and $N = 8$ modes (right) (see the caption of Fig. 2 for detailed explanation). The extracted parameters including their 95% confidence intervals in parenthesis are given above. **b**, Close-up of the measured MI.